CHAPTER 4

Transmission Mechanism of Wearable Devices Using the Human Body as a Transmission Channel

Koichi Ito, Masaharu Takahashi, and Katsuyuki Fujii

4.1 Introduction to Communications Using Circuits in Direct Contact with the Human Body

In recent years, the development of the information and communication devices, such as cellular phones, personal digital assistants (PDAs), digital video cameras, pocket video games, and so forth, has been progressing rapidly. This evolution gives increased convenience to our daily lives. In the near future, these appliances will begin to be attached to our body, in the form of wearable computers that can be connected to internal and external network systems [1]. However, [2] notes that there is currently no method for these personal devices to directly exchange data. We would like to exchange the data in the wearable devices without any physical constraints, such as external wire connections that may be easily tangled. The solution for networking these personal devices has been proposed as PANs that use the human body as a transmission channel [2, 3]. One of the merits of this system is that data can be exchanged by our natural actions, such as simply touching the receiver, and the user can be clearly aware of connection. Figure 4.1 shows the future applications. We can use these transmission systems for security, electronic money, amusement, and so forth.

Although many studies have been made on the development of wearable devices using the human body as a transmission channel, little is known about the transmission mechanism of such devices in the physical layer, from the viewpoint of the interaction between the electromagnetic wave and the human body [2–14]. Electromagnetic communication trials using the human body as a transmission medium have been carried out for more than a decade. However, most of the research has been conducted by researchers who just want to utilize the results, and until recently the physical mechanisms have not been studied.

This chapter investigates the transmission mechanisms of the wearable devices using the human body as a transmission medium [15–23]. Figure 4.2 shows the communication system [9] of the PAN using a 10-MHz carrier frequency [24]. When a user wearing the transmitter touches the electrode of the receiver, a trans-

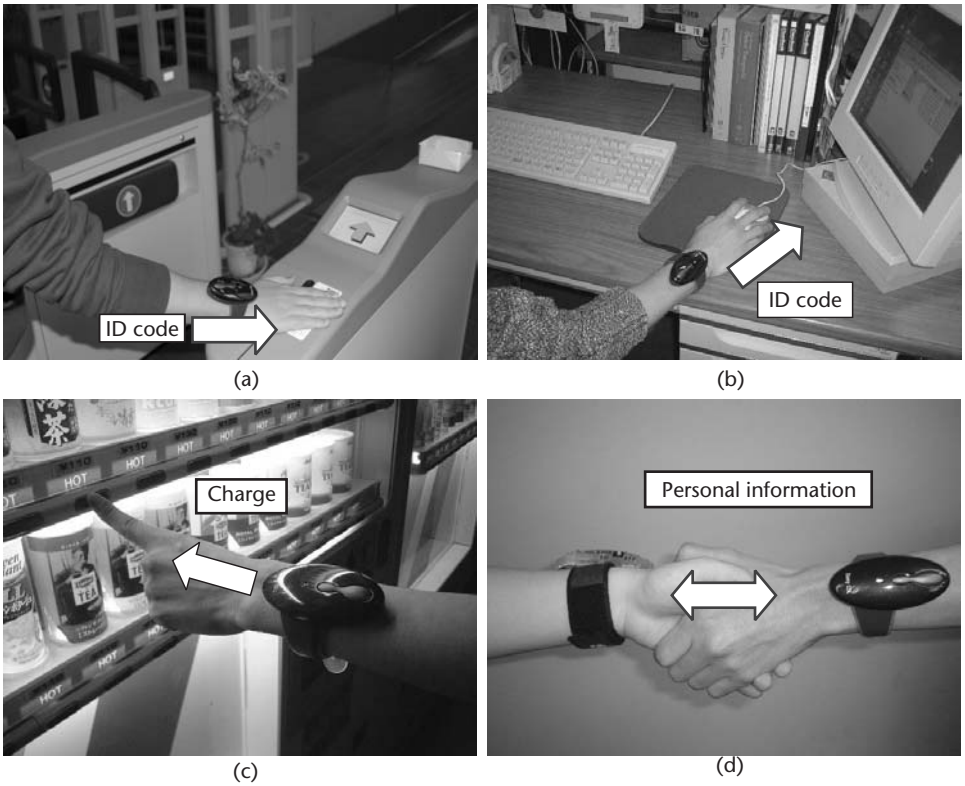

Figure 4.1 Examples of the future applications of PANs: (a) auto lock door, (b) auto login, (c) electronic money, and (d) amusement.

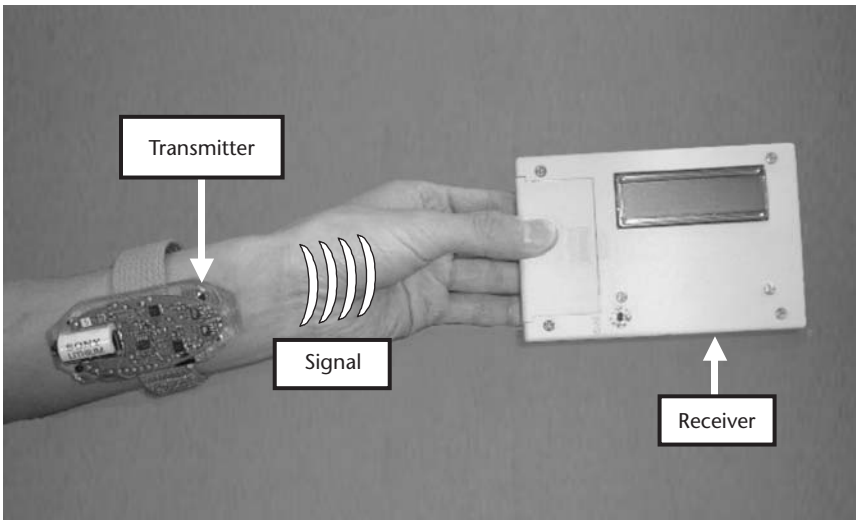

Figure 4.2 Transmission system using the human body as a transmission channel [9].

mission channel using the human body is formed. In this case, the receiver recognizes the user's ID, which can be personalized. This communication system uses the near-field region of the electromagnetic wave generated by the device, which is even-

tually coupled to the human body by electrodes. The structure of electrodes is one of the key issues for transmission using the human body.

In this chapter, the authors clarify the transmission mechanism of the wearable device using the human body as a transmission channel, from the viewpoint of the interaction between electromagnetic waves and the human body, by using computer simulations and by experiments on a biological tissue-equivalent solid phantom.

In Section 4.2, some calculation models of the transmitter attached to the human body are proposed, using the FDTD method [25, 26] to clarify the transmission mechanism. In the first step, the electric field distributions inside and outside of realistic high-resolution whole-body voxel models of a Japanese adult male and female of average height and weight [27] are investigated. The transmission system described in this chapter uses a 10-MHz carrier frequency, so the wavelength, $\lambda =$ 30m. A whole body calculation area will be needed because the human body may resonate at this frequency. As a result, there is no difference between the electric fields of a male and a female. Moreover, from the viewpoint of computer resources (memory, calculation time, and so forth), the calculation area can be limited to only the arm region, because most of the electric field is concentrated near the tip of the arm.

In the next step, only the arm models are used to simplify the calculation. The calculation models are a male arm, a female arm, and a rectangular parallel-piped homogeneous (muscle) arm that almost imitates the averaged-sized Japanese from finger to elbow [28], respectively. From these results, the authors conclude that the simple homogeneous arm model is sufficient to evaluate the electric field distribution of the human body, although it does not include skin, fat, bone, and so forth.

In the third step, the effective electrode structure is proposed to send the signal from the transmitter to the receiver. The differences of the distributions of the electric field are shown from the viewpoints of impedance matching theory by introducing the equivalent circuit models [29].

In Section 4.3, calculation results are compared to the measured results by using a biological tissue-equivalent solid phantom [30] to show the validity of the calculation. In the first step, each direction (rectangular coordinate) of the current distribution inside the arm is investigated, in order to understand the transmission mechanism. However, it is difficult to directly measure the current distribution inside the human body. It is inferred from measuring the magnetic field distribution close to the human body by using Ampère's law. In order to clarify the validity of the measurement, the measured magnetic field strength is compared to the calculated one. The result indicates a good agreement between measurement and calculation.

In the second step, a portable receiver, which was made by K. Fujii under Mr. S. Tajima's (Sony CSL) instructions, is introduced. This receiver can measure the received signal voltage directly without connecting outer measurement equipment, such as an oscilloscope, which would affect the measurement results. By attaching the receiver to the tip of the arm, electric field distributions and received signal levels are investigated. The reason for discussing the electric field distribution is that the received signal voltage of the receiver is calculated from the electric field. The argument from the viewpoint of the electric field is essential. From these results, the effective direction of electrodes of the transmitter to use the human body as a transmission channel is proposed.

In Section 4.4, after the validity of the calculation model was demonstrated in the previous section, the authors clarify the dominant signal transmission channel, because the question of whether the dominant signal channel is inside or outside the arm still remains unsettled. To answer this question, the calculation model of the arm wearing the transmitter and the receiver placed into a hole of a conductor plate is proposed. The electric field distribution and received signal voltage are investigated as a function of the gap between the hole of the conductor plate and the surface of the arm, when the signal passed through the hole in the conductor plate. If the dominant signal channel is outside the arm, then the received signal is not generated when the gap between the conductor plate and surface of the arm does not exist. On the other hand, if the dominant signal channel is inside the arm, then the received signal is generated in the same condition.

In Section 4.5, the authors conclude their studies concerning the transmission mechanism of the wearable devices using the human body as a transmission channel.

4.2 Numerical Analysis and Equivalent Circuit Models

4.2.1 Whole Body Models

Studies of wearable computers have recently attracted much public attention. It is thought that computing in the near future will be mainly performed through the interaction between wearable computers and ubiquitous computers. The communication system that uses the human body as a transmission channel has been proposed as one of these studies. When a user wearing the transmitter shown in Figure 4.3 touches the electrode of the receiver, a transmission channel is formed via the human body. The transmitter has two electrodes. One is the signal electrode fed by an excitation signal ($3V_{p\text{-}p}$, 10 MHz, sinusoidal wave), and the other is the ground (GND) electrode that is connected to the ground level of the electric circuit.

Figure 4.4 shows the calculation model of the transmitter. The authors have focused on the modeling of the transmitter for the FDTD calculations, and there has been considerable validity in that result [16, 20]. Two electrodes and circuit boards are modeled as perfect electric conductors. A continuous sinusoidal wave ($3V_{p\text{-}p}$, 10 MHz) is fed to the signal electrode.

In our study, the transmitter uses a 10-MHz carrier frequency, and its wavelength λ is much longer than the height of the human body. In order to investigate the coupling between the transmitter and the human body, full-scale human models are utilized. Figure 4.5 shows the realistic high-resolution whole-body voxel models of a Japanese adult male and female of average height and weight. According to [27], the male is 22 years old, is 172.8 cm tall, and weighs 65.0 kg. The female is 22 years old, is 160.0 cm tall, and weighs 53.0 kg. The resolution of these calculation models is $2 \times 2 \times 2$ mm. By putting these calculation models into the FDTD method, the electric field distributions inside and outside the whole bodies are investigated. The relative permittivity and conductivity of each tissue are equal to the value at 10 MHz [31]. The transmitter is attached to the wrist of the left arm. The size of the cells is $\Delta x = \Delta y = \Delta z = 2$ mm. The absorbing boundary condition is

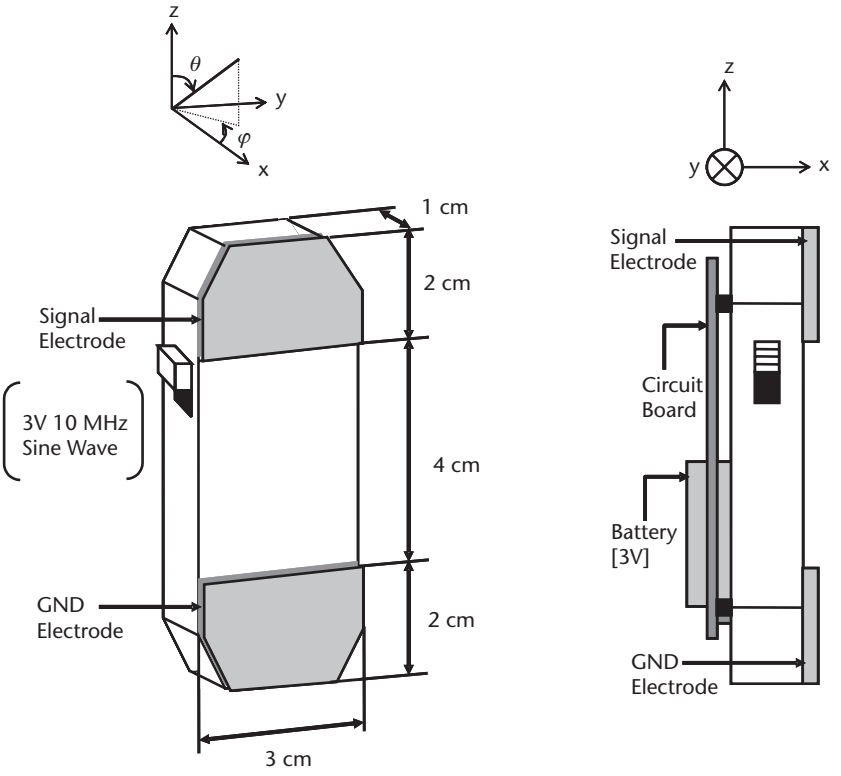

Figure 4.3 Wearable transmitter.

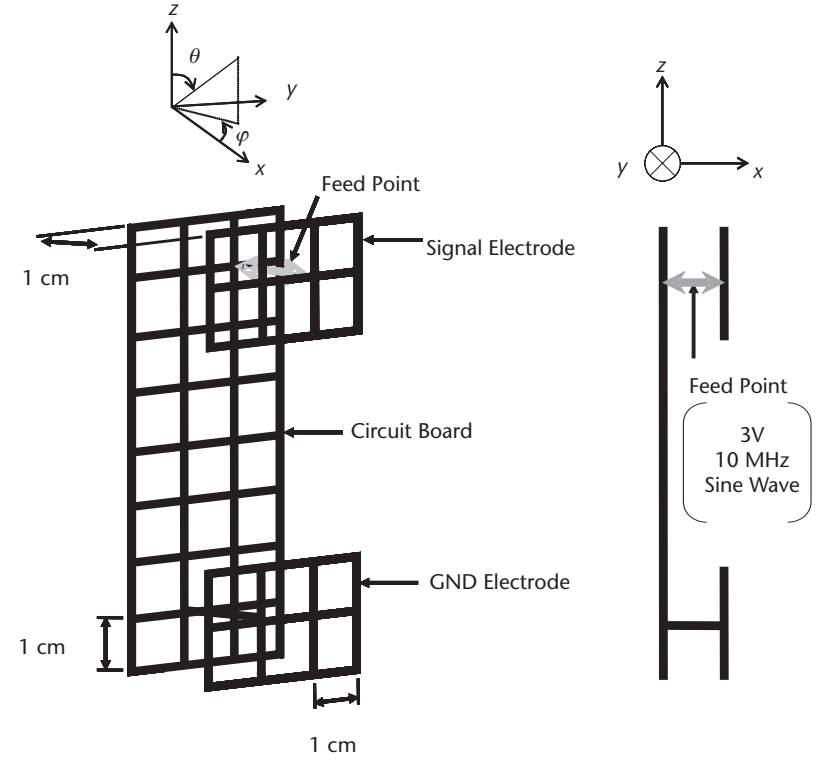

Figure 4.4 FDTD calculation model of the transmitter.

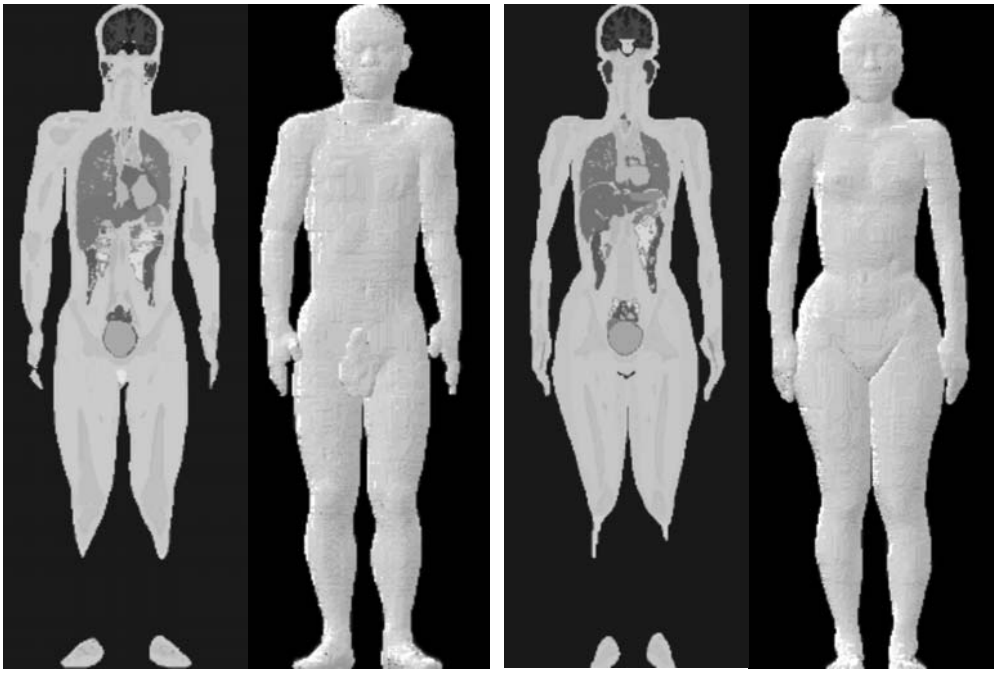

(a) (b)

Figure 4.5 Realistic high-resolution whole-body models of a Japanese adult: (a) male, and (b) female [27].

assumed to be Mur's second order, and the time step is 3.84 ps, satisfying the Courant stability condition.

Figure 4.6 shows the electric field distributions inside and outside the whole body of the male and the female. The observation plane includes the feeding point of the transmitter. From these results, it can be seen that most parts of the electric field are concentrated around the tip of the arm. Thus, only the arm model is sufficient to analyze the transmission between transmitter and receiver from the viewpoint of the computer resources (calculation time, memory, and so forth). Moreover, this system has an advantage over those using airborne radio waves from the viewpoint of energy consumption. As a result, this communication system that uses the human body as a transmission channel is useful for personal area networks. In the next section, the differences in the transmission properties caused by the electrode structure will be considered in detail by using only the arm model.

4.2.2 Arm Models

In this section, only the arm model is used, which simplifies the calculation. The electric field distributions inside and outside the arms are calculated. The calculation models are a male arm, a female arm, and a rectangular parallel-piped homogeneous (muscle) arm that almost imitates the averaged-sized Japanese arm from finger to elbow [28]. The size of the cells is $\Delta x = \Delta y = \Delta z = 2$ mm. The absorbing boundary condition is assumed to be Mur's second order, and the time step is 3.84 ps, satisfy-

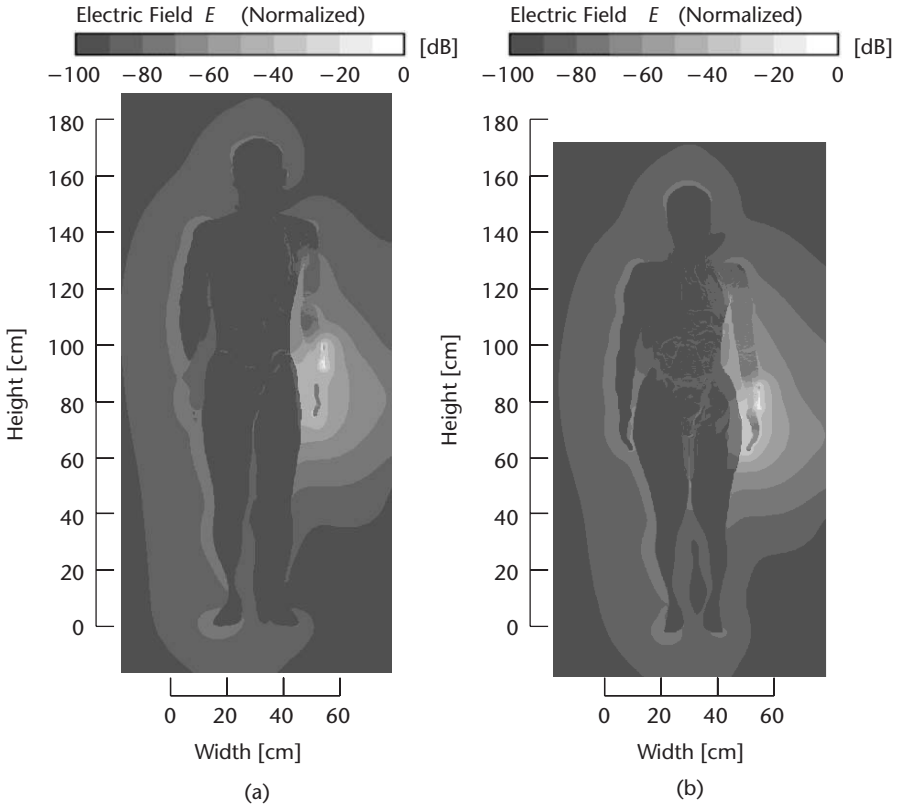

Figure 4.6 Electric field distributions inside and outside the whole body: (a) male, and (b) female.

ing the Courant stability condition. Figure 4.7(a) shows the electric field distribution of the cross section of the male arm. The observation plane includes the feeding point of the transmitter, and the value of the electric field is normalized by the electric field strength at the feeding gap. The electric field is propagated along the length of the arm. Most parts of the electric field are concentrated at the position of the transmitter. This transmission system using the human body as a transmission channel has the advantage of sending the signal merely by touching the electrode of the receiver. It is also advantageous from the viewpoint of the security, because the signal is not radiated into the air but propagated along the length of the arm. Figure 4.7(b) shows the electric field distribution of the cross section of the female arm. The electric field distribution is almost the same as Figure 4.7(a), although the shape and thickness of the arm are different. Figure 4.7(c) shows the simplest calculation model, which is a rectangular parallel-piped homogeneous (muscle) arm. The electric field distributions of Figure 4.7(c) inside and outside the arm are almost the same as those of Figure 4.7(a, b), in spite of a homogeneous structure, not including items such as skin, fat, bone, and so forth, which have different electrical parameters. From these results, it can be concluded that the simplest calculation model in Figure 4.7(c) is sufficient to evaluate the electric field distribution of the human body. After this section, the rectangular parallel-piped homogeneous (muscle) arm is utilized to simplify the discussion on transmission properties.

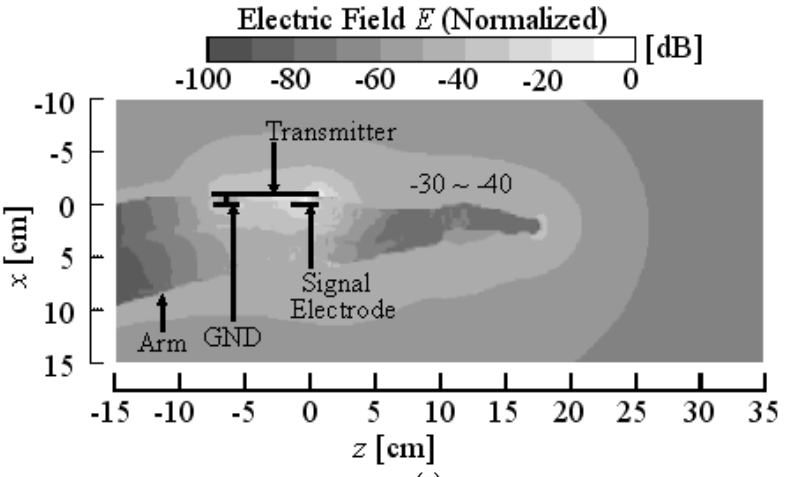

(a)

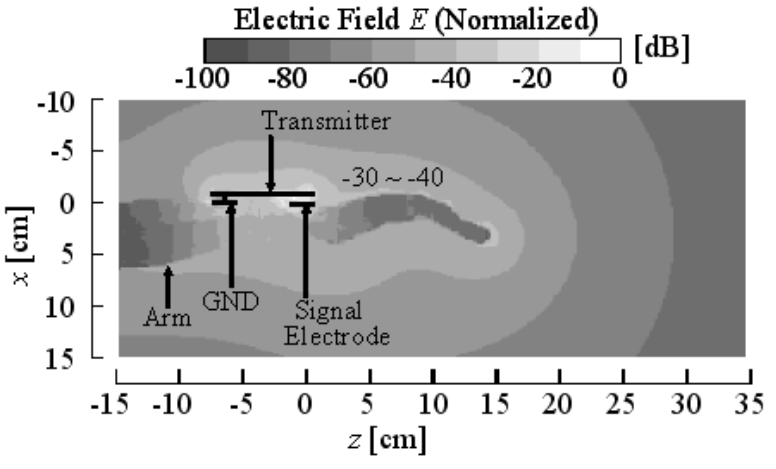

(b)

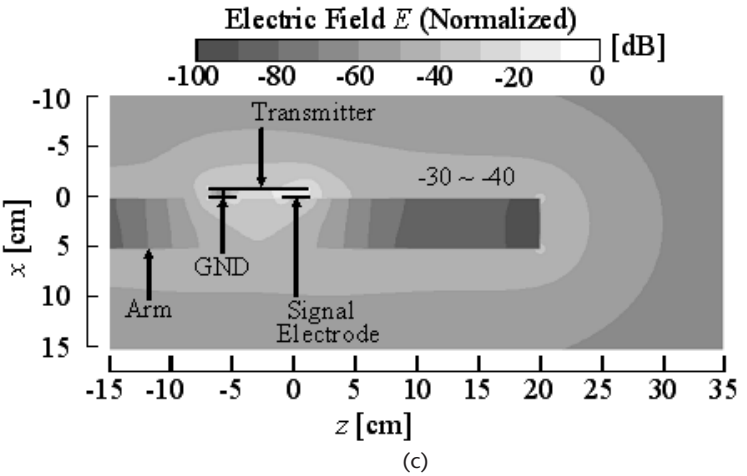

(c)

Figure 4.7 Electric field distributions inside and outside the arm: (a) male, (b) female, and (c) homogeneous model (muscle).

4.2.3 Effective Electrode Structure

This section examines the effective electrode structure of the transmitter for using the human body as a transmission channel. To investigate the electric field difference due to the electrode structure, two types of the electrode structures are introduced. Figure 4.8 shows the calculation model of the arm with the transmitter. Figure 4.8(a) shows the electrode model with the GND electrode, and Figure 4.8(b) shows the electrode model without the GND electrode. The arm is modeled as a rectangular parallel-pipe (5 × 5 × 45 cm), and the electrical parameters are equal to those of the muscle (relative permittivity $\varepsilon_r = 170.73$, and conductivity $\sigma = 0.62$ S/m) [32]. The size of the cells is $\Delta x = \Delta y = \Delta z = 1$ cm. The absorbing boundary condition is assumed to be Mur's second order, and the time step is 19.2 ps, satisfying the Courant stability condition.

Figure 4.9 shows the result of the electric field distributions inside and outside the arm. The observation plane is the x-z plane at $y = 0$, and 0 dB indicates the strength of the electric field at the feeding point. Figure 4.9(a) shows that the electric field is distributed along the surface of the arm (approximately from –30 to –40 dB), because the current path is formed between the signal electrode and the GND electrode. However, in Figure 4.9(b), level of the electric field on the surface of the arm

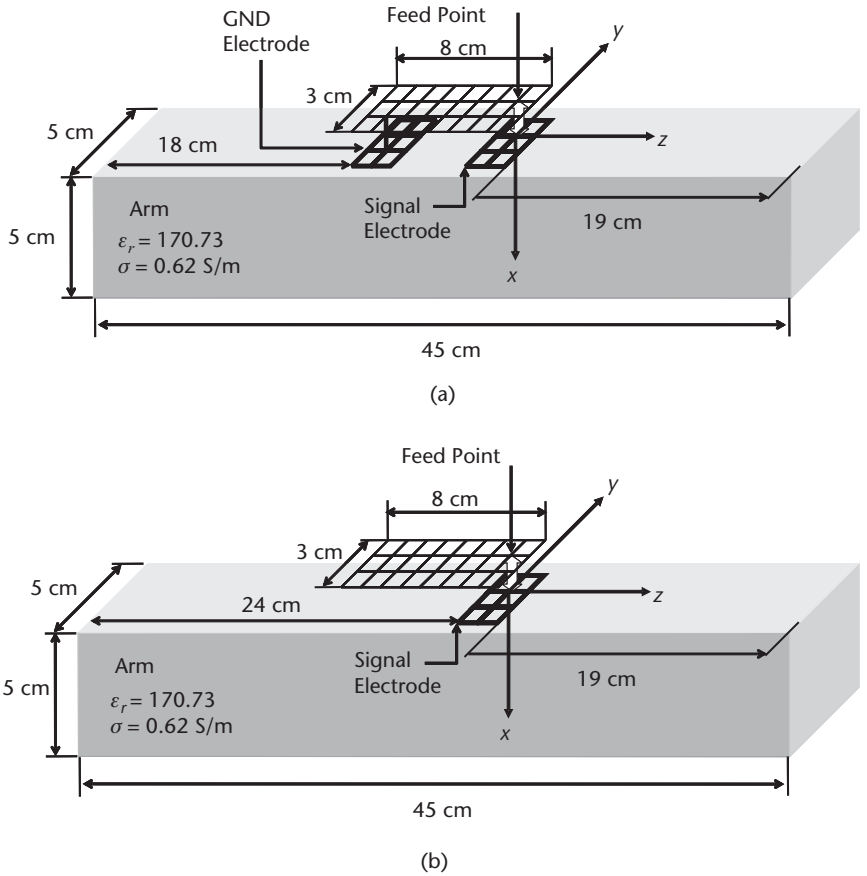

Figure 4.8 Calculation model of the arm wearing the transmitter: (a) Tx with GND electrode, and (b) Tx without GND electrode.

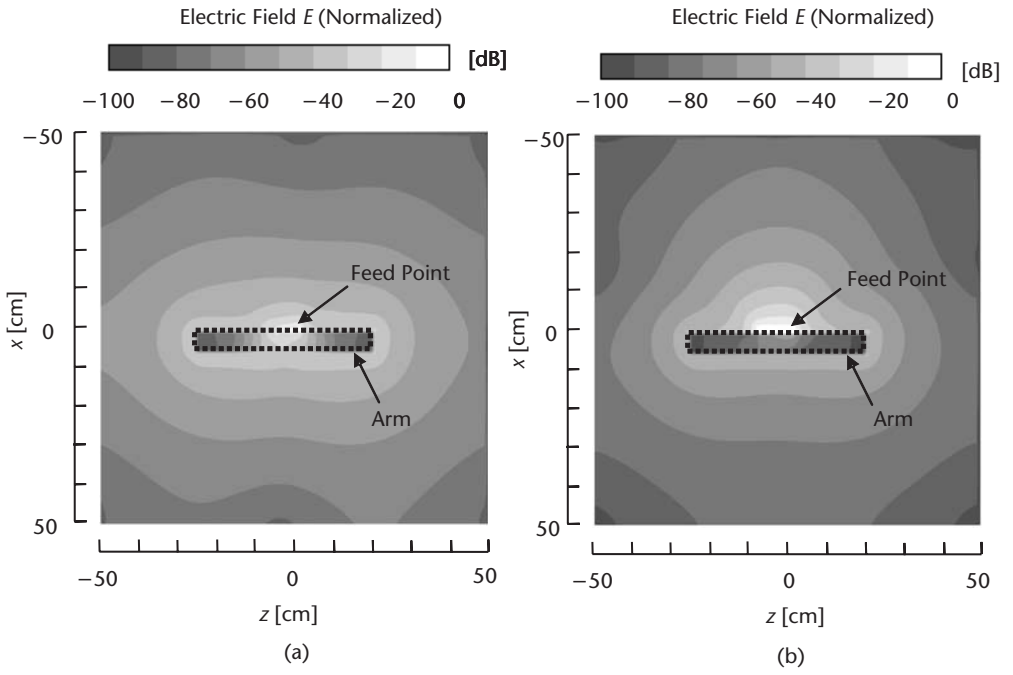

Figure 4.9 Electric field distributions inside and outside the arm: (a) Tx with GND electrode, and (b) Tx without GND electrode.

seems low (approximately from −40 to −50 dB), and the electric field does not penetrate inside the arm. Therefore, the GND electrode is necessary to generate the electric field around the arm. Next, this result will be investigated by using the equivalent circuit models of power transmission.

4.2.4 Equivalent Circuit Models

In this section, the differences of the electric field distributions in Figure 4.9 are investigated by using the equivalent circuit models [29]. Figure 4.10 shows the equivalent circuit models of the transmitter attached to the arm. Input power is expressed as the following equation:

$$P_{\text{in}} = \frac{1}{2}\text{Re}\left\{Z_{\text{in}} \cdot \frac{V_g}{Z_g + Z_{\text{in}}} \cdot \frac{V_g^*}{\left(Z_g + Z_{\text{in}}\right)^*}\right\} = \frac{1}{2}\frac{\left|V_g\right|^2 \cdot \text{Re}\left(Z_{\text{in}}\right)}{\left|Z_g + Z_{\text{in}}\right|^2} = P_{\text{av}} S \tag{4.1}$$

where V_g, Z_g, Z_{in}, and P_{av} are the supply voltage, the output impedance, the input impedance, and the available power, respectively. If Z_g is equal to Z_{in}, then Figure 4.10 represents a transmission line that is matched, and $S = 1$. Therefore, P_{av} and S are expressed as the following equations.

$$P_{\text{av}} = \frac{\left|V_g\right|^2}{8\text{Re}\left(Z_g\right)} \tag{4.2}$$

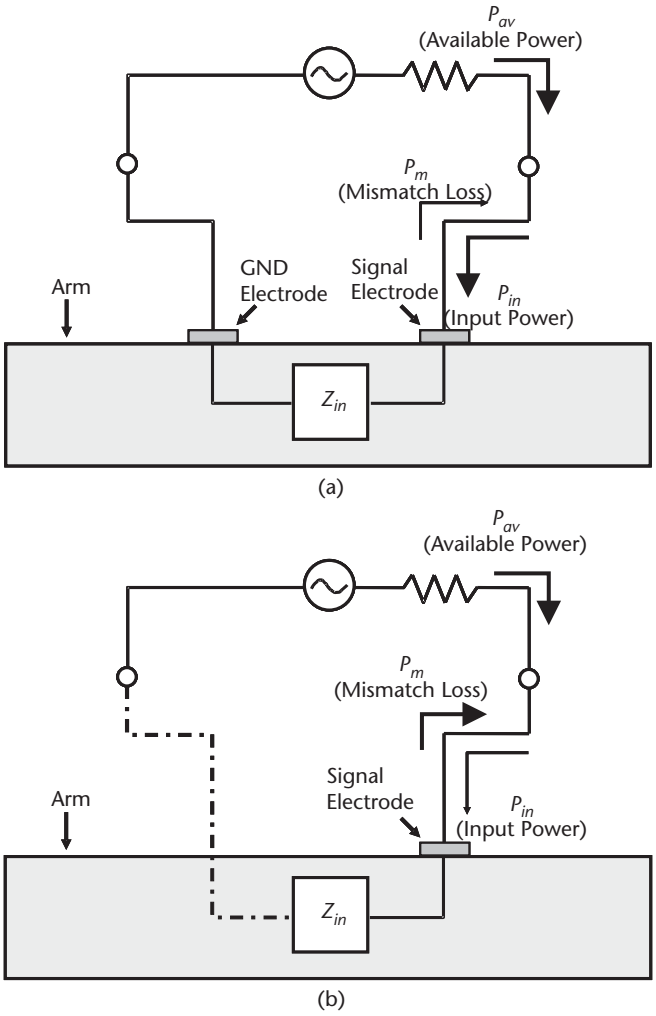

Figure 4.10 Equivalent circuit models: (a) Tx with GND electrode, and (b) Tx without GND electrode.

$$S = \frac{4\mathrm{Re}\left(Z_g\right)\cdot\mathrm{Re}\left(Z_{\mathrm{in}}\right)}{\left|Z_g + Z_{\mathrm{in}}\right|^2} \tag{4.3}$$

Under the assumption that the resistance of the electrode can be neglected, total power of the loss and the radiation efficiency based on the available power are expressed as follows:

$$P_t = P_b + P_m \tag{4.4}$$

$$\eta = \frac{P_r}{P_{\mathrm{av}}} = \frac{P_{\mathrm{av}} - P_t}{P_{\mathrm{av}}} \tag{4.5}$$

where P_b, P_m, and P_r are the absorption power of the human body, the mismatch loss, and the radiation power, respectively.

By using the FDTD calculation, the input impedance Z_{in} [Ω], the input power P_{in} [W], and the radiation power P_r [W] can be calculated. Table 4.1 shows the partition of the available power P_{av}, where $P_{av} = P_{in} + P_m$, under the assumption that the output impedance of the equivalent circuits are 50Ω, by substituting Z_{in}, P_{in}, and P_r for (4.1) to (4.5). From Table 4.1, the imaginary part of Z_{in} is low in the case of the GND electrode. Thus, most parts of the available power P_{av} are fed to the signal electrode, and change the absorption power of the human body P_b. On the other hand, in the case without the GND electrode, the input impedance Z_{in} has a large amount of capacitance, because the absence of the GND electrode causes stray capacitance between the human body and the transmitter. Thus, most of the available power P_{av} is lost as mismatch loss P_m. From these results, it can be concluded that existence of the GND electrode can be quite effective for signal transmission, because it enables impedance matching between the signal generator and the human body.

4.3 Experiments Using Human Phantom

4.3.1 Measurement of the Signal Distributions

A phantom is the material that has the same physical properties as biological tissues and the human body. Accurate measurements for the electromagnetic field distribution in the human body are conducted using various biological tissue-equivalent phantoms, such as liquid or solid phantoms, in which nonuniform models are applicable [33]. In this section, the current distributions inside the human body are measured by using the solid phantom that imitates the human arm introduced in Section 4.2, which shows the validity of the FDTD calculations. From these results, the optimal direction of the transmitter electrodes is used on the human body as a transmission channel. However, it is difficult to directly measure the current distribution inside the human body. Rather, it is inferred from measuring the magnetic field distribution close to the human body, by using Ampère's law. A shielded loop antenna with a diameter of 1 cm is used for the measurement.

Figure 4.11 shows the arrangement used to measure the various components of the magnetic field distribution. The transmitter has two electrodes. One is the signal

Table 4.1 Calculated Parameters of the Equivalent Circuits (10 MHz)

	With GND	*Without GND*
Z_{in} (Ω)	$37.92 - j4.598$	$13.56 - j2.835$
P_{av} (W)	5.625×10^{-3}	5.625×10^{-3}
S	9.784×10^{-1}	3.373×10^{-4}
P_{in} (W)	5.508×10^{-3}	1.898×10^{-6}
P_m (W)	1.212×10^{-4}	5.623×10^{-3}
P_b (W)	5.499×10^{-3}	1.684×10^{-6}
P_r (W)	4.613×10^{-6}	2.128×10^{-7}
η	8.201×10^{-4}	3.783×10^{-5}
	$\left(P_{av} = P_{in} + P_m \quad P_{in} = P_b + P_r\right)$	

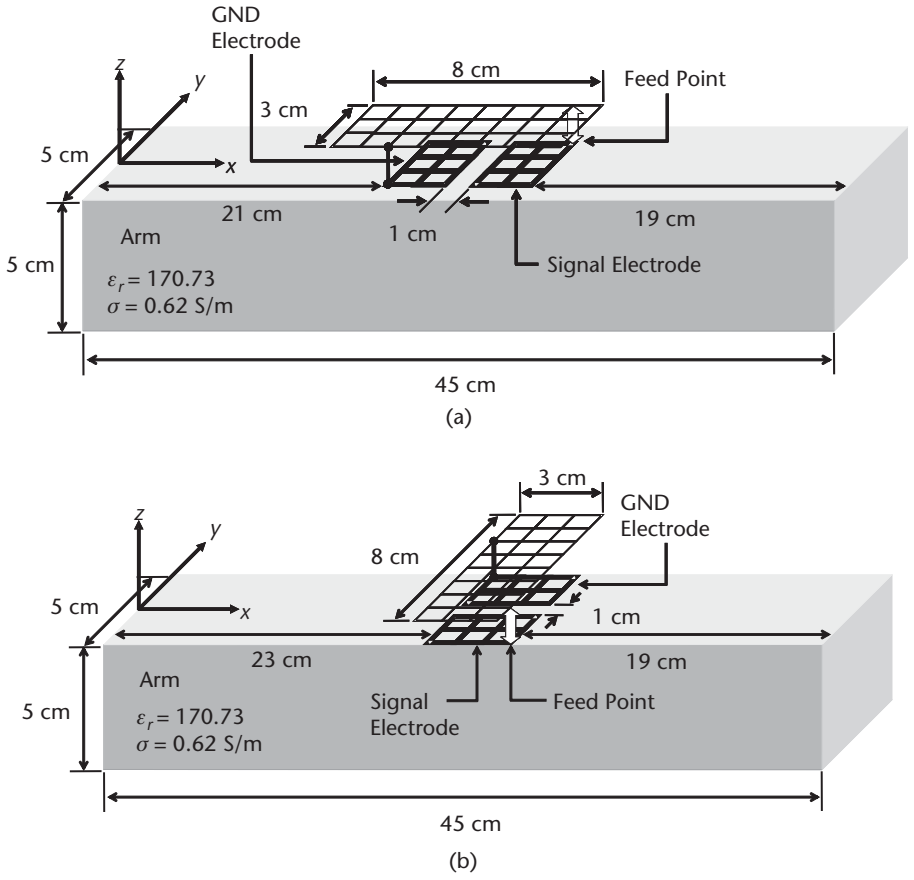

Figure 4.11 Direction of the transmitter: (a) longitudinal direction, and (b) transversal direction.

electrode to feed an excitation signal ($3V_{p\text{-}p}$, sinusoidal wave of 10 MHz), and the other is the GND electrode that is connected to the ground level of the electrical circuit. The direction of the transmitter changes according to two patterns to compare the magnetic field distributions. One pattern is the longitudinal direction shown in Figure 4.11(a), and the other pattern is the transversal direction shown in Figure 4.11(b). In addition, the conventional distance between the signal electrode and the GND electrode was 4 cm. However, its distance is reduced to 1 cm, so as to be less than the width of the arm. The experimental muscle-equivalent phantom used for the arm, which is modeled by a rectangular parallel-pipe ($5 \times 5 \times 45$ cm), has relative permittivity $\varepsilon_r = 81$ and conductivity $\sigma = 0.62$ S/m. Although the relative permittivity of the muscle at 10 MHz equals 170.73 [32], the authors have verified that they can use this phantom [20], because the received signal voltage is almost the same, and there is great difficulty in making a phantom with such a high relative permittivity. Moreover, in Section 4.2, the electric field distribution around the whole body model wearing the transmitter was investigated, and it was found that the electric field is concentrated around the arm. Hence, an arm model without the whole body can be used.

Figure 4.12 shows the experimental setup for enhanced measurements. For the shielded loop antenna, a coaxial cable and a copper wire with a diameter of 1.6 mm

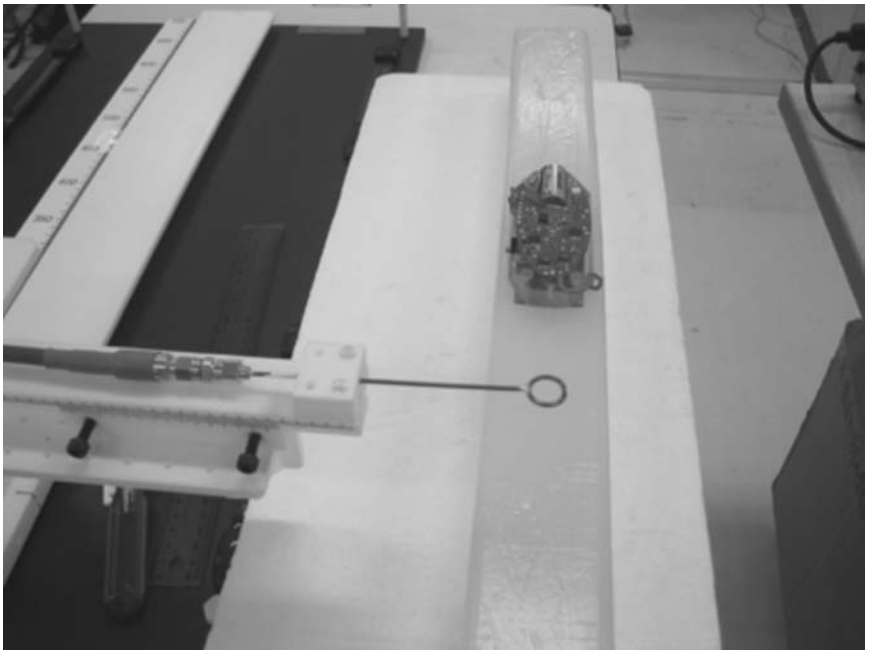

Figure 4.12 Setup for measurement (longitudinal direction).

are used. At the tip of the antenna, a 0.5-mm gap is constructed to generate the received signal voltage. A spectrum analyzer and a power amplifier are also used. The shielded loop antenna is set 3 cm above the surface of the arm, and the magnetic field distributions are measured along the *x- axis at* $y = 0$ and $z = 3$ cm.

Figure 4.13 shows the various components of the magnetic field distribution around the arm with the transmitter. The level of each point is normalized by the value of H_z at $x = 26$ cm in Figure 4.13(b), which is the maximum value of all measured data in Figure 4.13. In the case of the transmitter set to the longitudinal direction in Figure 4.13(a), from Ampère's law, the dominant current distribution inside the arm is the x component, because the H_y component is stronger compared to the H_x and H_z components near the tip of the arm ($x = 30$ to 45 cm). In the case of the transmitter attached to the transversal direction in Figure 4.13(b), the dominant current distribution inside the arm is the y component, because the H_x and H_z components are stronger than the H_y components near the tip of the arm ($x = 30$ to 45 cm). Therefore, it can be concluded that the direction of the dominant current distribution inside the arm is the same as the direction of the electrodes of the transmitter, because the current is formed between the signal electrode and the GND electrode.

4.3.2 Comparison Between Measurement and Calculation

Figures 4.14 and 4.15 indicate the comparison between measured and simulated magnetic fields to show the validity of the measurements and the FDTD calculations. These figures show the transmitter set to the longitudinal direction and transversal direction, respectively. In the FDTD calculation, two electrodes and circuit boards of the transmitter are modeled as perfect conductor sheets. The sizes of the electrodes are 2 × 3 cm, and the size of the circuit board is 8 × 3 cm. The numer-

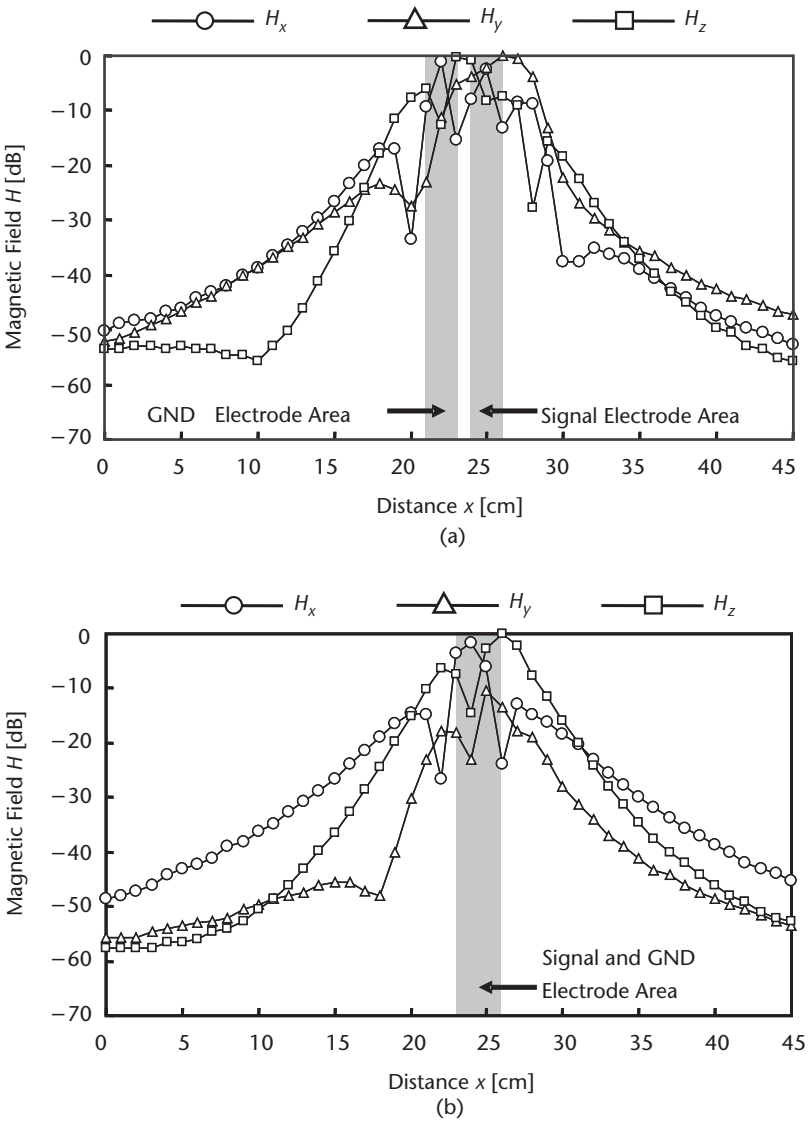

Figure 4.13 Measured magnetic field distributions around the arm: (a) transmitter in the longitudinal direction, and (b) transmitter in the transversal direction.

ical muscle-equivalent phantom used for the arm has relative permittivity $\varepsilon_r = 170.73$, and conductivity $\sigma = 0.62$ S/m. The size of the cells is $\Delta x = \Delta y = \Delta z = 1$ mm. The absorbing boundary condition is assumed to be Mur's second order, and the time step is 1.92 ps, satisfying the Courant stability condition. In Figures 4.14 and 4.15, all the simulated data are normalized by the value of H_x at $x = 24.5$ cm in Figure 4.15(a), which is the maximum value of all the simulated data in Figures 4.14 and 4.15. To discuss the difference between the measured and calculated magnetic fields, the following equation is defined:

$$\text{Difference} = \sqrt{\frac{1}{x_2 - x_1}\int_{x_1}^{x_2}\left\{H_{Meas.}(x) - H_{FDTD}(x)\right\}^2 dx} \tag{4.6}$$

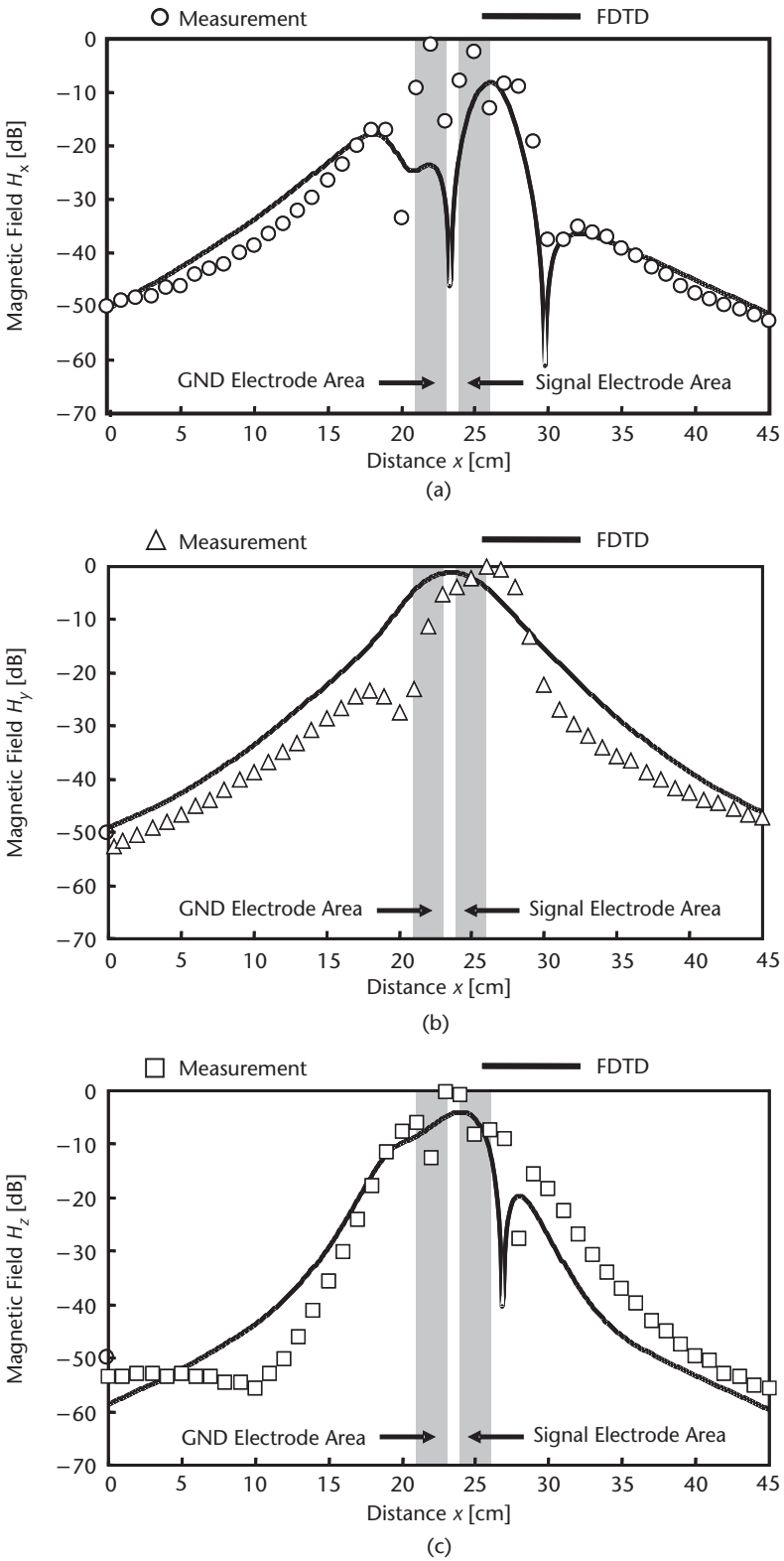

Figure 4.14 Comparison between measured and calculated magnetic field in the longitudinal direction: (a) H_x component, (b) H_y component, and (c) H_z component.

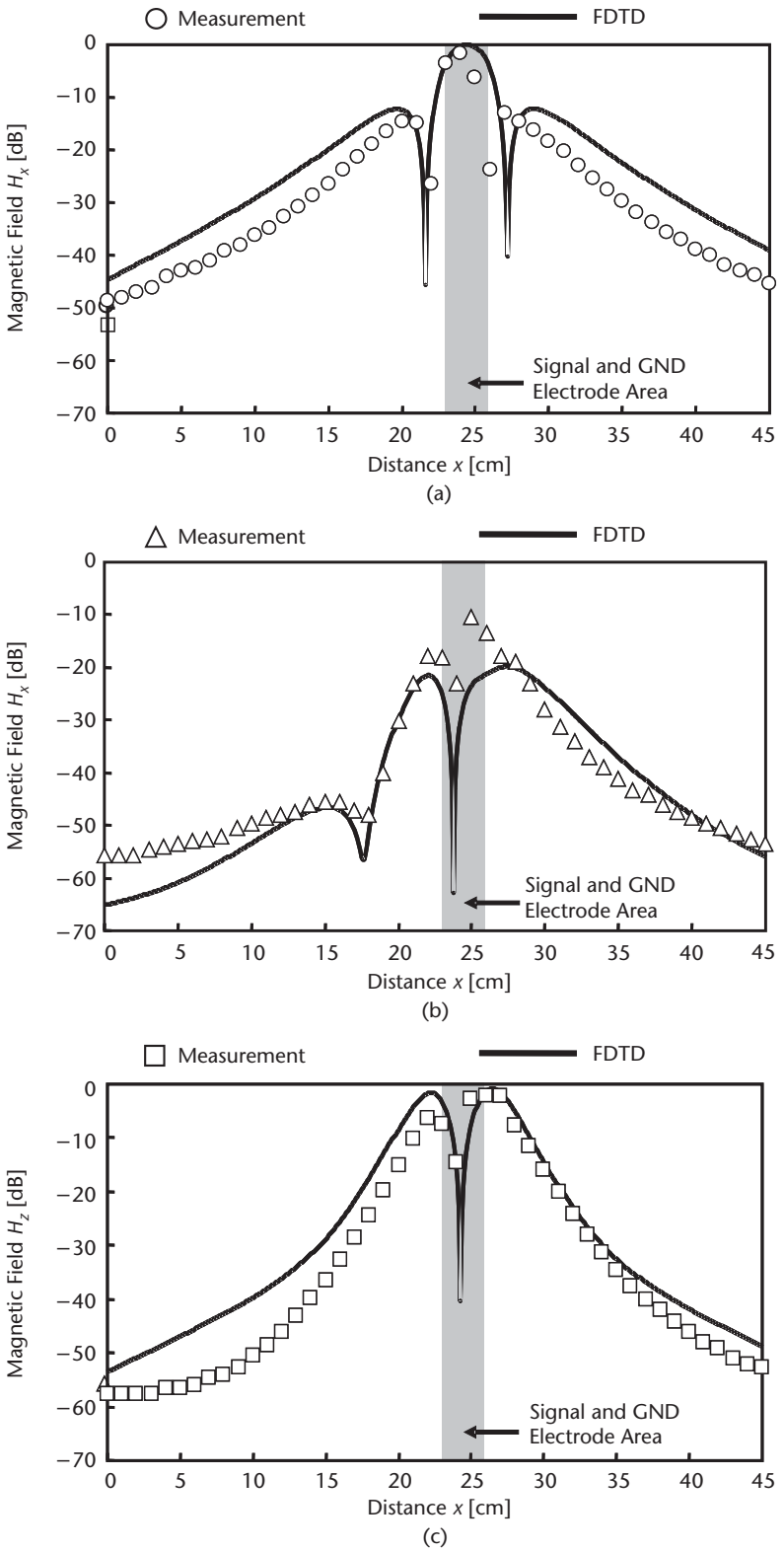

Figure 4.15 Comparison between measured and calculated magnetic field in the transversal direction: (a) H_x component, (b) H_y component, and (c) H_z component.

where $H_{\text{Meas.}}(x)$ and $H_{\text{FDTD}}(x)$ indicate the measured and calculated magnetic fields, respectively. x_2 and x_1 equal 45 cm and 0 cm, respectively. Table 4.2 shows the difference between $H_{\text{Meas.}}(x)$ and $H_{\text{FDTD}}(x)$, using (4.6). From Table 4.2, all the differences of Figures 4.14 and 4.15 are almost less than 7 dB. These differences may be caused by the dynamic range for the measurement being limited to approximately -55 dB. However, the rate of decrease and the null point as a function of the distance x is generally in agreement. From this viewpoint, each component of the magnetic field distribution can be compared, and this supports the validity of the measurements and the FDTD calculations.

4.3.3 Electric Field Distributions in and Around the Arm

Figure 4.16 illustrates the electric field distributions (root-sum-square) of both directions of the electrodes of the transmitter. The reason for discussing the electric field distribution is that the received signal voltage of the receiver is calculated from the electric field. Thus, the argument from the viewpoint of the electric field is essential. The structure of the receiver is illustrated in Figure 4.17. The receiver has a receiving electrode and an LCD that can directly indicate the received signal voltage. The reason for having no GND electrode on the receiver is that it reduces the received signal voltage [17]. There is no optimal direction of the receiver because the receiver has only one electrode. Figure 4.17(b) is the FDTD calculation model of the receiver. The receiving electrode and the circuit board are modeled as perfect electric conductors. The received signal voltage is calculated from the electric field at the receiving point. Therefore, this receiver does not detect the magnetic field, but only the electric field. The distance between the transmitter and receiver is fixed at 17 cm, because the transmitter is located at the center of the arm and the receiver is located at the tip of the arm. The observation plane is the x-z plane, including the receiving point of the receiver. The electric field is normalized to the value at the feeding gap. In the case of the longitudinal direction of the transmitter in Figure 4.16(a), the electric field is propagated along the surface of the arm (from -50 to -60 dB). However, in Figure 4.16(b), the level of the electric field on the surface of the arm seems low (from -60 to -70 dB), and the electric field is not propagated along the surface of the arm, but rather is radiated on the upper side of the arm. This result indicates a disadvantage for practical use, compared to Figure 4.16(a), in terms of higher signal reception. In addition, Figure 4.18 shows the electric field distributions without the arm. The loss of the electric field at the receiving point is quite large (< -80 dB) compared to the Figure 4.16. Therefore, it can be concluded that this transmission system uses the human body as a transmission channel.

Next is given an interpretation of the difference between the two parts of Figure 4.16. As shown in Figure 4.13(a), the dominant current distribution is the x compo-

Table 4.2 Difference Between Measured and Calculated Magnetic Field Distributions

	Figure 4.14			*Figure 4.15*		
	(a)	*(b)*	*(c)*	*(a)*	*(b)*	*(c)*
Difference (dB)	6.7	7.0	7.2	7.0	5.4	6.5

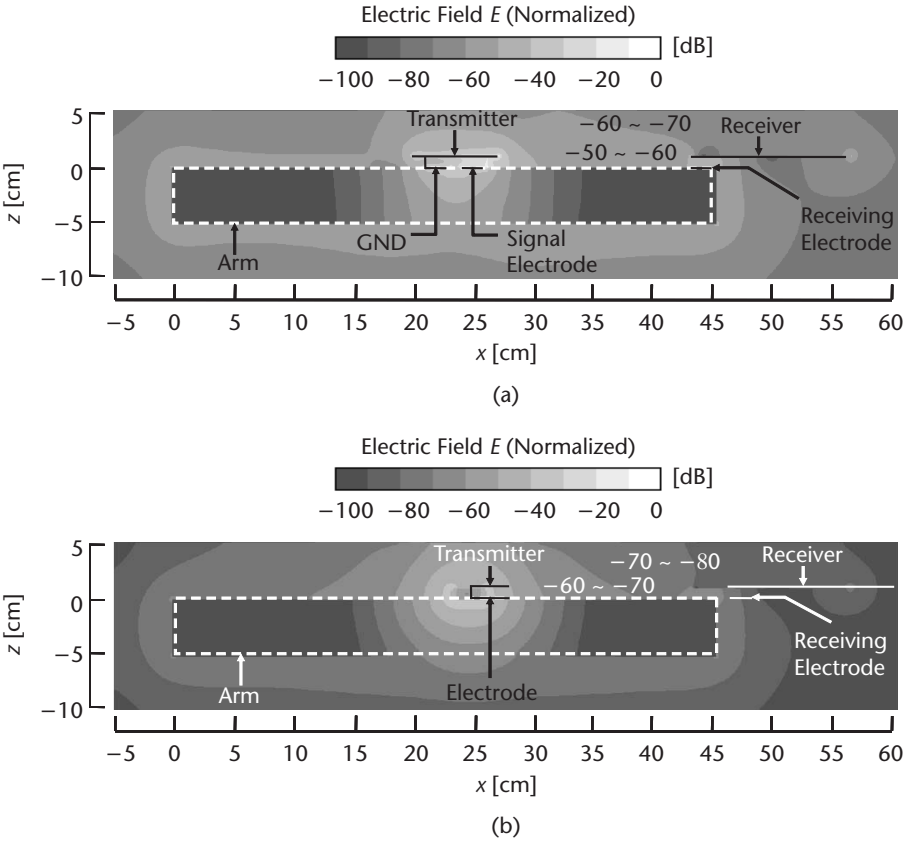

Figure 4.16 Electric field distributions in and around the arm: (a) transmitter in the longitudinal direction, and (b) transmitter in the transversal direction.

nent when the transmitter is set to the longitudinal direction. Thus, the electric field is distributed along the length of the arm (x direction). On the other hand, as shown in Figure 4.13(b), the dominant current distribution is the y component when the transmitter is set to the transversal direction. Thus, the electric field is not distributed along the x direction. The difference of the current distribution causes the difference of the electric field distribution.

4.3.4 Received Signal Voltage of the Receiver

Figure 4.19 shows the measurement arrangements for the received signal voltage according to the direction of the electrodes of the transmitter. In order to verify the validity of the calculation models, the received signal voltage is compared to the measured voltage by using the biological tissue-equivalent solid phantom. In Figure 4.19(a), the transmitter is attached in the longitudinal direction, while in Figure 4.19(b), the transmitter is attached in the transversal direction.

Figure 4.20 shows the comparison between the measured received signal voltages and the calculated voltages. Good agreement is noted, which supports the validity of both the FDTD model and measurement. When compared to the received signal voltage for the longitudinal direction, the transversal voltage drops by nearly

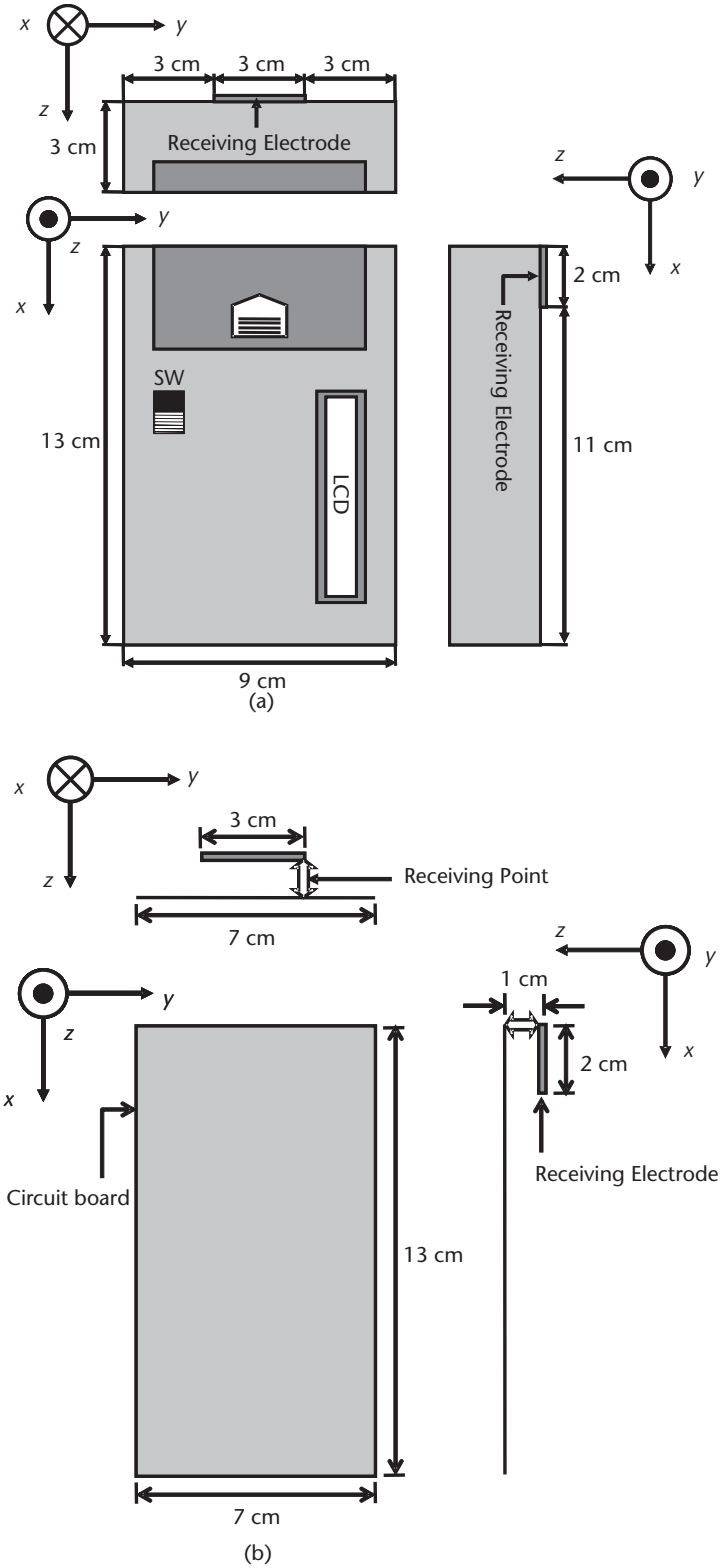

Figure 4.17 Structure of the receiver: (a) exterior of the receiver, and (b) FDTD calculation model.

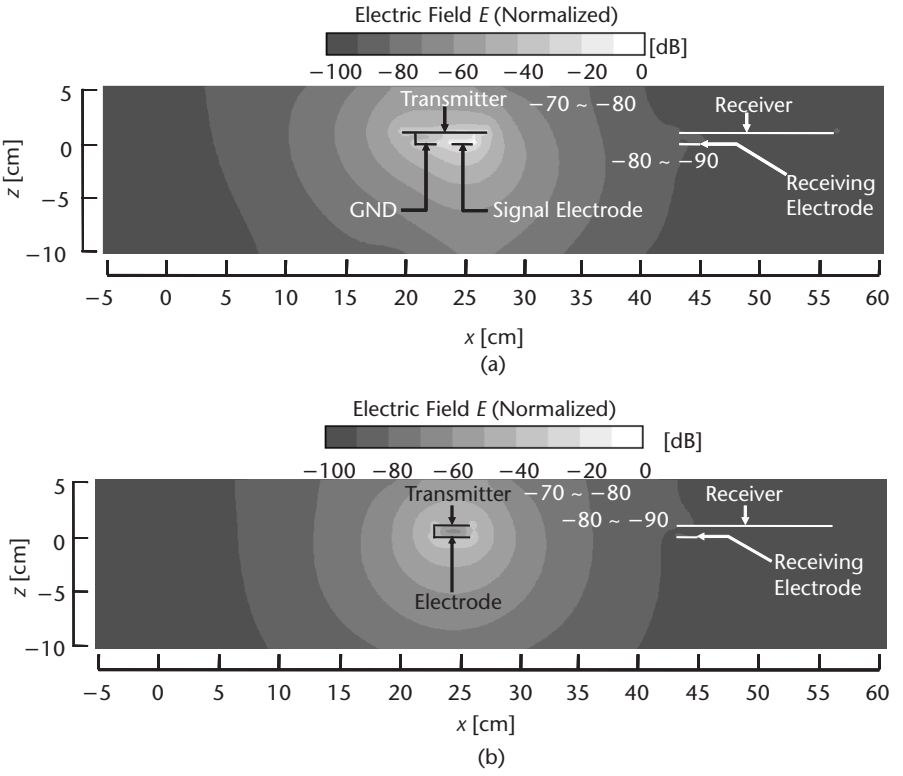

Figure 4.18 Electric field distributions without arm: (a) longitudinal direction, and (b) transversal direction.

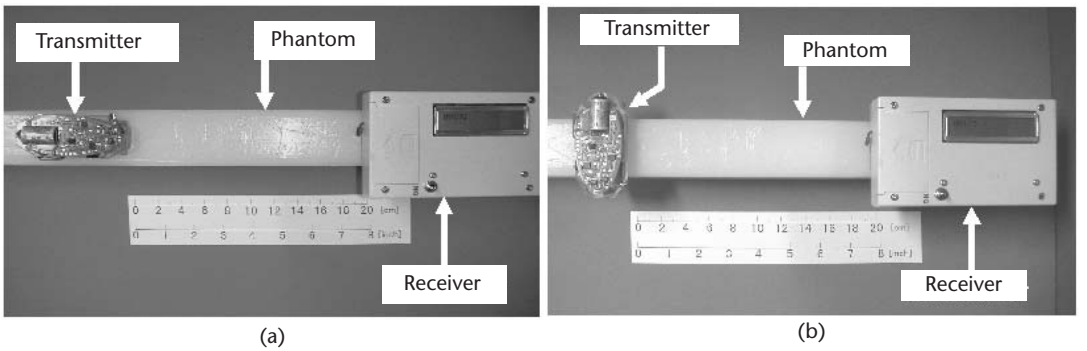

Figure 4.19 Measurement conditions of the received signal voltage: (a) longitudinal direction, and (b) transversal direction.

10%. The received signal voltages without the arm are almost zero. The transmission system using the human body as a transmission channel has an advantage over transmission systems using airborne radio waves. Regarding the difference of the relative permittivity, the received signal voltages are almost equal. It is appropriate to use the phantom with ε_r set to 81 as a substitute for a phantom with ε_r set to 170.73.

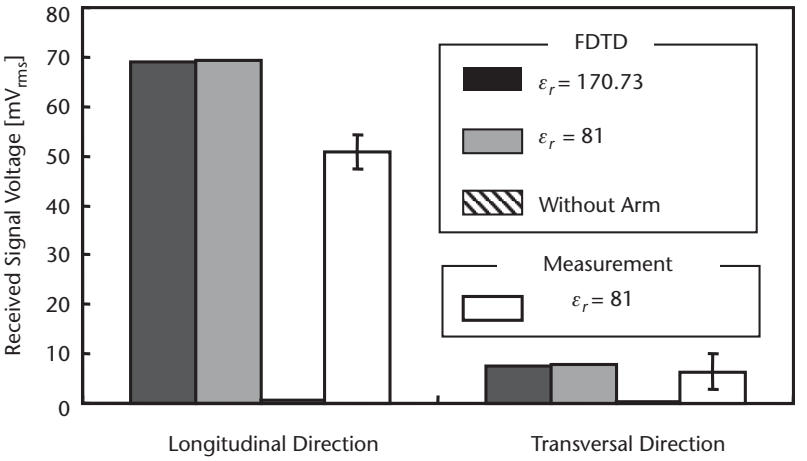

Figure 4.20 Received signal voltage.

In conclusion, the longitudinal direction is more effective for sending the signal to the receiver, as compared with the transversal direction. These investigations have made it clear that we can effectively use the human body as a transmission channel by guiding the current along the length of the arm.

4.4 Investigation of the Dominant Signal Transmission Path

4.4.1 Calculation Model

In this section, the dominant signal transmission channel is investigated, because the question of whether the dominant signal channel is inside or outside the arm still remains unsettled. To answer this question, the calculation model of an arm wearing the transmitter and the receiver placed into a hole of a conductor plate is proposed. Figure 4.21 shows the calculation model of the arm with the transmitter and receiver using the FDTD method. The reason for constructing such a calculation model is as follows. If the dominant signal transmission channel is inside the arm, then the received signal will be generated when the gap $g = 0$. On the other hand, if the dominant signal transmission channel is outside the arm, the electric field from the transmitter will not propagate toward the receiver, but will be reflected at the position of the conductor plate when the gap $g = 0$. The dominant signal transmission path can be clarified by using this calculation model. The size of the conductor plate d is physically infinity, because it is attached to the absorbing boundary of the FDTD. The size of the cells is $\Delta x = \Delta y = \Delta z = 1$ mm. The absorbing boundary condition is assumed to be Mur's second order, and the time step is 1.92 ps, satisfying the Courant stability condition. The distance between the signal electrode and the GND electrode is set to the conventional size (4 cm). By using this model, the electric field distribution and the received signal voltage are investigated as a function of the gap g between the hole of the conductor plate and the surface of the arm.

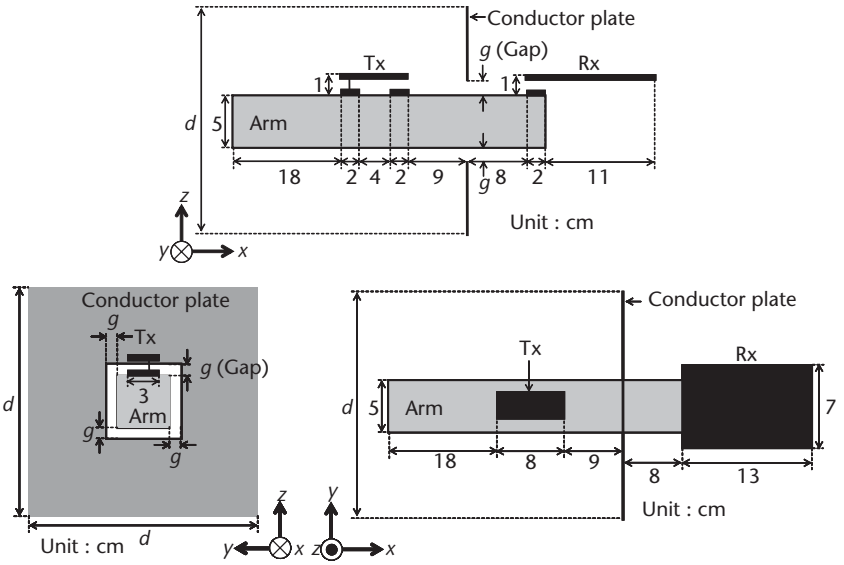

Figure 4.21 Calculation model to investigate the dominant signal transmission path.

4.4.2 Electric Field Distributions and Received Signal Voltages

Figure 4.22 illustrates the electric field distributions (root-sum-square) inside and outside the arm. The observation plane is the *x*-*z* plane, and the *y* plane includes the receiving point. The electric field is normalized to the value at the feeding gap. Figure 4.22(a, b) shows the electric field distributions when the gap *g* is −1 and 0 mm, respectively. It can be seen that the electric field is not propagated toward the receiver, but instead is reflected at the point of the conductor plate. However, in Figure 4.22(c–f), as the gap *g* between the conductor plate and the surface of the arm becomes wider, the electric field is propagated more toward the receiver.

Figure 4.23 shows the comparison between the measured received signal voltages and the calculated values as a function of the gap *g*. To measure the received signal voltages, the conductor plate with a size of 200 × 200 cm is used (d = 200 cm), as shown in Figure 4.24. When the size of the gap *g* ranges from −1 to 0 mm, the received signal voltage is almost zero. However, as the gap *g* between the conductor plate and the surface of the arm becomes wider, the received signal voltage rises sharply. The result shows a good agreement between the calculated and measured received signal levels, which indicates a considerable validity in both the FDTD and measurement. The reason for the difference of the received signal voltage between the longitudinal direction in Figure 4.20 and without the conductor in Figure 4.23 comes from the difference of the distance between the signal electrode and the GND electrode. In Figure 4.20, the distance between the signal electrode and the GND electrode is 1 cm. The circuit of the transmitter is almost shorted. Thus, the electric field generated from the transmitter is lower than the conventional size (4 cm).

On the basis of these results, the dominant signal transmission channel using the human body as a transmission channel is not inside the arm, but is on the surface of the arm, because the signal seems to be distributed as a surface wave.

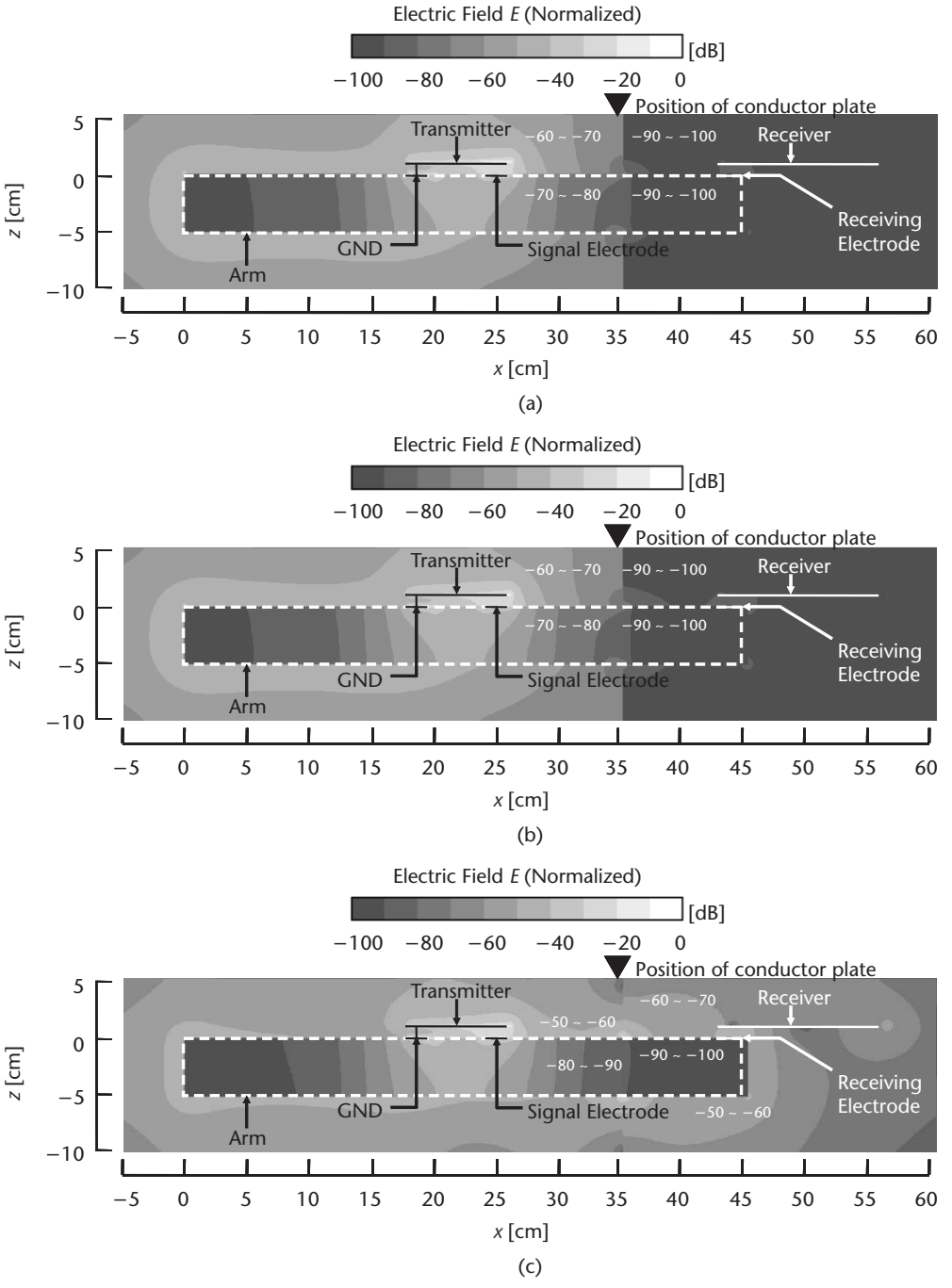

Figure 4.22 Electric field distributions inside and outside the arm wearing the transmitter and the receiver. (a) Gap $g = -1$ mm; (b) gap $g = 0$ mm; (c) gap $g = 1$ mm; (d) gap $g = 5$ mm; (e) gap $g = 10$ mm; and (f) without conductor plate.

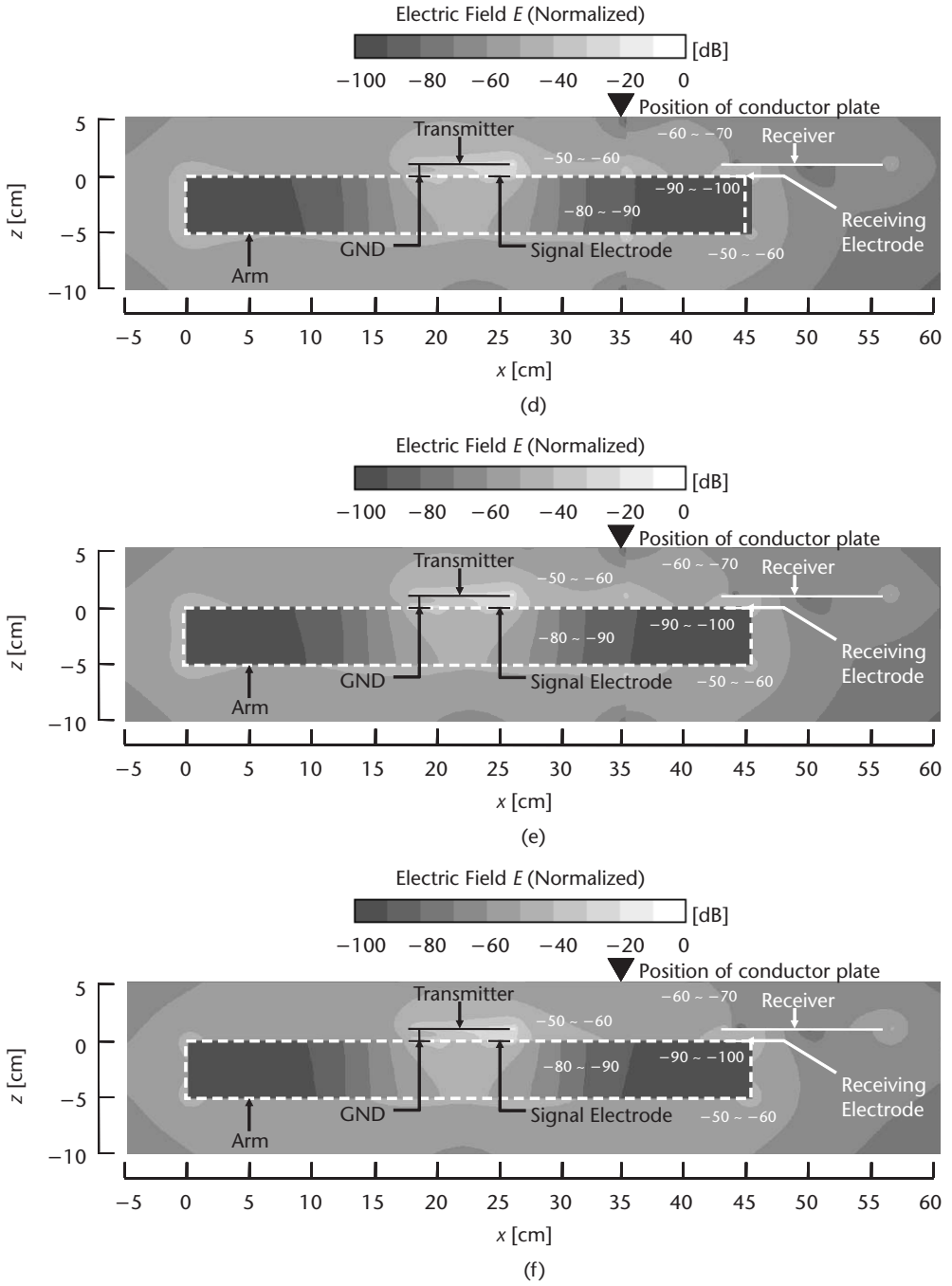

Figure 4.22 (continued.)

4.5 Conclusions

In this chapter, the authors have clarified the transmission mechanism of the wearable device using the human body as a transmission channel, from the viewpoint of the interaction between electromagnetic waves and the human body.

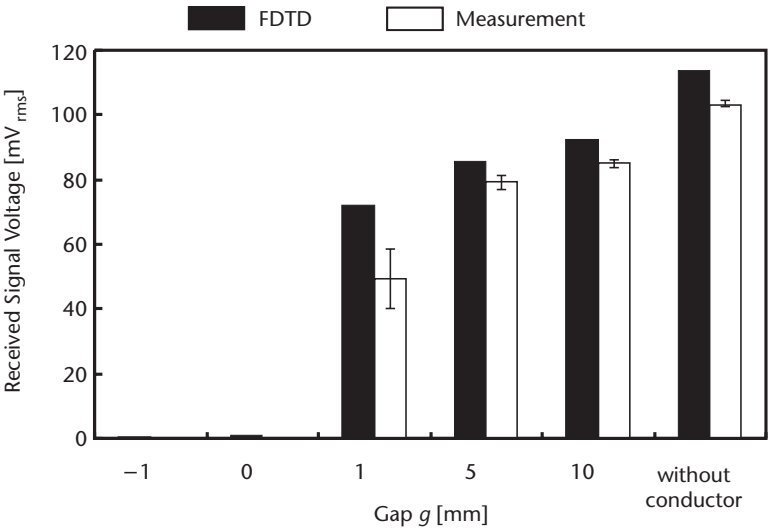

Figure 4.23 Received signal voltage as a function of the gap *g* between the conductor plate and surface of the arm wearing the transmitter and the receiver.

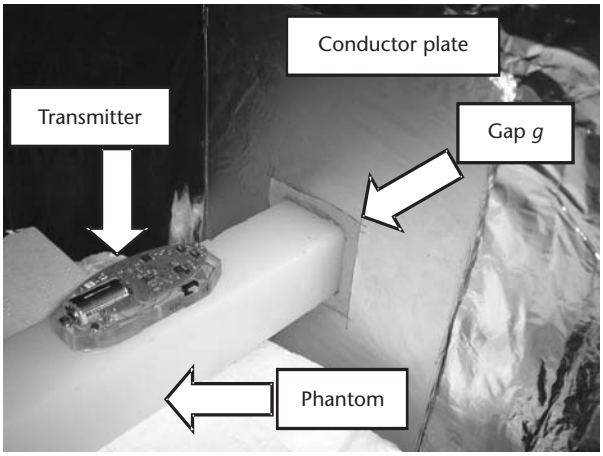

Figure 4.24 Measurement condition.

In Section 4.2, some calculation models and equivalent circuit models of the transmitter attached to the human body were proposed using the FDTD method. The difference in the electric field distributions due to the electrode structures of the transmitter was estimated. As a result, it was found that the GND electrode of the transmitter attached to the arm strengthens the generated electric field around the arm, because it enables impedance matching between the transmitter and the human body.

In Section 4.3, calculation results are compared to the measured results by using the biological tissue-equivalent solid phantom to show the validity of the calculation. Through the measurements, the distributions of the current flowing inside the arm

were inferred. The results showed a good agreement between the calculations and the measurements. Setting the two electrodes of the transmitter in the longitudinal direction of the arm is more effective than setting the electrodes in the transversal direction. These investigations have made it clear that we can effectively use the human body as a transmission channel by guiding the current along the length of the arm.

In Section 4.4, the dominant signal transmission channel was investigated, because the question of whether the dominant signal channel was inside or outside the arm still remained unsettled. The results lead us to the conclusion that the dominant signal transmission channel of a wearable device using the human body as a transmission channel is near the surface of the arm, because the signal seems to be propagated as a surface wave. However, there is still been room for theoretical arguments and further study about surface propagation of this result.

References

[1] Weiser, M., "The Computer for the Twenty-First Century," *Scientific American*, September 1991, pp. 66–75.

[2] Zimmerman, T. G., "Personal Area Networks (PAN): Near-Field Intra-Body Communication," M.S. thesis, Cambridge, MA: MIT Media Laboratory, September 1995.

[3] Zimmerman, T. G., "Personal Area Networks: Near-Field Intra-Body Communication," *IBM Systems J.*, Vol. 35, No. 3 & 4, 1996, pp. 609–617.

[4] IBM Web site, http://www.almaden.ibm.com/cs/user/pan/pan.html.

[5] Zimmerman, T. G., et al., "Applying Electric Field Sensing to Human-Computer Interfaces," *Proc. CHI'95*, May 1995, pp. 280–287.

[6] Post, E. R., et al., "Intrabody Buses for Data and Power," *Proc. ISWC'97*, October 1997, pp. 52–55.

[7] Fukumoto, M., and Y. Tonomura, "Body Coupled FingeRing: Wireless Wearable Keyboard," *Proc. ACM CHI'97*, March 1997, pp. 147–154.

[8] Handa, T., et al., "A Very Low-Power Consumption Wireless ECG Monitoring System Using Body as a Signal Transmission Medium," *Proc. 1997 Int. Conference on Solid-State Sensors and Actuators*, Chicago, IL, 1997, pp. 1003–1006.

[9] Matsushita, N., et al., "Wearable Key: Device for Personalizing Nearby Environment," *Proc. 4th Int. Symp. Wearable Computers* (*ISWC 2000*), October 2000, pp. 119–126.

[10] Doi, K., et al., "Development of the Communication Module Used Human Body as the Transmission Line," *Proc. Human Interface Symp. 2001*, 2001, pp. 389–392 (in Japanese).

[11] Hachisuka, K., et al., "Development of Wearable Intra-Body Communication Devices," *Sensors and Actuators A: Physical*, Vol. 105, No. 1, 2003, pp. 109–115.

[12] Shinagawa, M., et al., "A Near-Field-Sensing Transceiver for Intra-Body Communication Based on the Electro-Optic Effect," *Proc. Instrumentation and Measurement Technology Conference*, May 2003, pp. 296–301.

[13] NTT redtacton Web site, http://www.redtacton.com/.

[14] Matsushita Electric Works Technology: press release (2004.09.13), http://www.mew.co.jp/e-press/2004/0409-02.htm.

[15] Fujii, K., K. Ito, and S. Tajima, "Signal Propagation of Wearable Computer Using Human Body as Transmission Channel," *Proc. 2002 Interim Int. Symp. Antennas and Propagation*, Yokosuka Research Park, Japan, November 2002, pp. 512–515.

[16] Fujii, K., K. Ito, and S. Tajima, "A Study on the Modeling of Communication System Using Human Body as Transmission Channel," *J. of the Institute of Image Information and Television Engineers* (*ITE*), Vol. 56, No. 11, November 2002, pp. 1845–1849 (in Japanese).

[17] Fujii, K., K. Ito, and S. Tajima, "A Study on the Receiving Signal Level in Relation with the Location of Electrodes for Wearable Devices Using Human Body as a Transmission Channel," *Proc. 2003 IEEE Int. Symp. Antennas and Propagation and USNC/CNC/URSI North American Radio Science Meeting*, Columbus, OH, June 2003, pp. 1071–1074.

[18] Fujii, K., and K. Ito, "Evaluation of the Received Signal Level in Relation to the Size and Carrier Frequencies of the Wearable Device Using Human Body as a Transmission Channel," *Proc. 2004 IEEE AP-S Int. Symp. Antennas and Propagation and USNC/URSI National Radio Science Meeting*, Vol. 1, Monterey, CA, June 2004, pp. 105–108.

[19] Fujii, K., et al., "Study on the Optimal Direction of Electrodes of a Wearable Device Using the Human Body as a Transmission Channel," *Proc. 2004 Int. Symp. Antennas and Propagation*, Vol. 2, Sendai International Center, Japan, August 2004, pp. 1005–1008.

[20] Fujii, K., K. Ito, and S. Tajima, "A Study on the Calculation Model for Signal Distribution of Wearable Devices Using Human Body as a Transmission Channel," *IEICE Trans. on Commun.*, Vol. J87-B, No. 9, September 2004, pp. 1383–1390 (in Japanese).

[21] Fujii, K., et al., "A Study on the Relation Between Surface Wave Component and Received Signal Level of the Wearable Device Using the Human Body as a Transmission Channel," *Proc. 2004 Korea-Japan Joint Conference on AP/EMC/EMT*, Seoul, Korea, November 2004, pp. 271–274.

[22] Fujii, K., et al., "Study on the Transmission Mechanism for Wearable Device Using the Human Body as a Transmission Channel," *IEICE Trans. on Commun.*, Vol. E88-B, No. 6, June 2005, pp. 2401–2410.

[23] Fujii, K., et al., "A Study on the Frequency Characteristic of a Transmission Channel Using Human Body for the Wearable Devices," *Proc. 2005 Int. Symp. Antennas and Propagation*, Vol. 2, Seoul, Korea, August 2005, pp. 359–362.

[24] Sony Computer Science Laboratories, Inc. Web site: http://www.csl.sony.co.jp/index.shtml.

[25] Yee, K. S., "Numerical Solution of Initial Boundary Value Problems Involving Maxwell's Equations in Isotropic Media," *IEEE Trans. on Antennas and Propagation*, Vol. AP-14, No. 3, 1966, pp. 302–307.

[26] Uno, T., *Finite Difference Time Domain Method for Electromagnetic Field and Antenna Analyses*, Tokyo: Corona Publishing, 1998 (in Japanese).

[27] Nagaoka, T., et al., "Development of Realistic High-Resolution Whole-Body Voxel Models of Japanese Adult Male and Female of Average Height and Weight, and Application of Models to Radio-Frequency Electromagnetic-Field Dosimetry," *Physics in Medicine and Biology*, Vol. 49, 2004, pp. 1–15.

[28] "Human Body Dimensions Data for Ergonomic Design," *Report of National Institute of Bioscience and Human Technology*, Vol. 2, No. 1, 1994.

[29] Ogawa, K., Y. Koyanagi, and K. Ito, "An Analysis of the Effective Radiation Efficiency of the Normal Mode Helical Antenna Close to the Human Abdomen at 150 MHz and Consideration of Efficiency Improvement," *Electronics and Communications in Japan, Part 1*, Vol. 85, No. 8, 2002, pp. 23–33.

[30] Matsuda, T., *Hyperthermia Manual*, Tokyo: Magbross Press, 1991, pp. 155–156 (in Japanese).

[31] FCC Web site, http://www.fcc.gov/fcc-bin/dielec.sh.

[32] IFAC Web site, http://niremf.ifac.cnr.it/tissprop/.

[33] Okano, Y., et al., "The SAR Evaluation Method by a Combination of Thermographic Experiments and Biological Tissue-Equivalent Phantoms," *IEEE Trans. on Microwave Theory and Techniques*, Vol. 48, No. 11, November 2000, pp. 2094–2103.